*Mon. Not. R. astr. Soc.* (1990) **242**, 241–249

# Starbursts superimposed on old populations: spectral evolution of the composite system over $3 \times 10^9$ yr

E. Bica,[1] D. Alloin[2] and A. Schmidt[1,3]

[1]*Universidade Federal do Rio Grande do Sul, Departamento de Astronomia, Av. Bento Gonçalves, 9500, 91500 Porto Alegre, RS, Brazil*
[2]*Observatoire de Paris, Section de Meudon, DAEC, F-92195 Meudon, France*
[3]*Universidade Federal de Santa Maria, Departamento de Matematica/NEPAE, Faixa de Camobi, km 5, 97100 Santa Maria, RS, Brazil*

Accepted 1989 June 22. Received 1989 May 23; in original form 1989 January 30.

## SUMMARY

We simulate in this paper the occurrence of star formation events superimposed on old populations, during the last $3 \times 10^9$ yr, by combining star cluster integrated spectra of different ages with those of red strong-lined galaxy nuclei. As the young star clusters have metallicities in the range $-0.5 < [Z/Z_\odot] \leqslant 0$, our simulations address in particular the case of starbursts induced by galaxy interactions bringing fresh, low-metallicity gas to the host galaxy. We follow the evolution of the composite spectrum for burst to old population mass ratios of 10, 1 and 0.1 per cent. We present also the effects of the starburst on the restframe *BVRI* magnitudes and colours, as well as on the equivalent widths ($W_\lambda$) for a set of metallic and Balmer lines. If a burst amounts to 10 per cent of the galaxy mass, the underlying old population of the galaxy will remain undetectable, even in the near infrared, during $5 \times 10^7$ yr. When this strong burst reaches intermediate ages ($10^9$ yr $< t < 5 \times 10^9$ yr) it still contributes $\approx 20$ per cent of the total visible flux. For a 1 per cent mass burst, the underlying galaxy should be marginally detectable, in terms of near-infrared absorption features, during the H II region phase. However, because of the *a priori* unknown burst duration, any attempt to identify the old population by means of integrated observations will be difficult owing to the prompt occurrence of the red supergiant phase. At intermediate ages, the 1 per cent mass burst has become barely visible. Finally a 0.1 per cent mass burst affects the galaxy spectrum during $2 \times 10^7$ yr only. It is virtually inconspicuous in the visible and near-infrared ranges as soon as $t \geqslant 10^8$ yr. We discuss a series of spectral configurations of interest, whenever the burst and galaxy contributions are of comparable importance, depending on the burst age and strength. These results hold true in the more general frame of star formation, and are not restricted to interaction-induced events.

## 1 INTRODUCTION

Bursts of star formation are observed in a variety of sites among which are interacting galaxies or the surroundings of active galactic nuclei (e.g. Wright *et al.* 1988 and references therein). They are prominent in some classes of objects such as the blue compact galaxies (Searle, Sargent & Bagnuolo 1973; Lequeux *et al.* 1979; Thuan 1983). Starbursts also appear to power the large infrared luminosity of most *IRAS* galaxies (Lonsdale, Persson & Matthews 1984; Dennefeld, Karoji & Belford 1985). In order to understand the burst-inducing processes in these objects better, it is important to quantify the relative fractions of young and old populations. This in turn will provide clues to the origin of the gas consumed in the star formation event. Other important questions relate to the evolution of the burst-galaxy system, or to the time it will take for a given burst to become inconspicuous within its host galaxy. Burst simulations constitute a powerful tool with which to answer these questions.

The effects of star formation bursts on *UBV* colours of galaxies have been extensively discussed by Larson & Tinsley (1977). They used an evolutionary code in which starburst galaxies were represented by the sum of two population components, one old and one young. The latter study, as well as other burst simulations (e.g. Searle *et al.* 1973; Arimoto & Tarrab, private communication) provide broad-band colour predictions. In the present paper, in addition to broad-band magnitudes, we show detailed spectral simula-

tions which can be directly compared to starburst galaxy spectral observations. Our approach also differs from the previous ones in the sense that we use real star clusters and real galaxy nuclei as elements for the combinations. The very first million year evolution of a burst of star formation has recently been studied at length, both observationally and theoretically (e.g. Terlevich 1985). Our study is complementary to such an analysis because it follows the evolution of the burst up to a few gigayears and its relative importance at every stage with respect to the underlying old population.

We have recently built up a library of star cluster integrated spectra in the visible and near-infrared ranges and a corresponding grid of spectral properties as a function of age and metallicity (Bica & Alloin 1986a, hereafter BA86a; BA86b; BA87b). We have also analysed spectra of galaxy nuclei from morphological types E to Sc, in the luminosity range $-23.3 \leqslant M_B \leqslant -16.6$ (BA87a; BA87b). A new method for stellar population synthesis, using the grid of star cluster spectral properties has been presented in Bica (1988). This method has the advantage over conventional ones, which use stellar libraries, of having two parameters: age and metallicity. In addition, the population synthesis becomes less dependent on theoretical assumptions, as both the initial mass function and stellar evolution are implicit in the real star cluster observations. We do assume, however, that the initial mass functions in the base star clusters are similar to those in starbursts. Results are given as the flux proportions from each component represented in the base by the two parameters (age, metallicity). There remains the problem of relating flux fractions to mass fractions. To do this, the photometric evolution of a single generation system – a star cluster – has been analysed by Arimoto & Bica (1989) using the evolutionary code developed by Arimoto & Yoshii (1986). Fine grids in age and stellar mass intervals were employed in the star cluster evolution model. The resulting evolution of the mass to light ratio, $M/L_v$, was studied by Bica, Arimoto & Alloin (1988), allowing the mutual transformation of population synthesis results from flux to mass fractions.

In the current paper, we simulate the present-day appearance of star-forming events superimposed on old populations, which have occurred over the last $3 \times 10^9$ yr. This is achieved by combining elements of the star cluster and galaxy spectral libraries. A star cluster of a given age represents the starburst while a red strong-lined galaxy nucleus stands for a typical old metal-rich underlying population. The scope of this study is thus star formation from fresh, low-metallicity gas ($\leqslant Z_\odot$) in massive galaxies, as could result from galaxy interactions; burst simulations in old metal-poor systems such as dwarf elliptical galaxies will be discussed in a forthcoming paper. The flux proportions for combining the spectra are dictated by three burst-to-galaxy mass ratios, namely 10, 1 and 0.1 per cent. In Section 2 we provide details of the simulation building and we discuss star formation events. We compute in Section 3 the *BVRI* magnitudes and the colours of the resulting galaxy plus burst systems, as a function of the burst age and strength (burst-to-galaxy mass ratio). Similarly, we give in Section 4 the $W_\lambda$ for a set of metallic and Balmer lines. The real situations these models can describe and the conclusions of this work are given in Section 5.

**Table 1.** Properties of the star cluster spectral groups.

| Group | Age ($10^9$ yr) | M/L$_V$ | L$_V$/L(5870 Å) | L(5870 Å) |
|---|---|---|---|---|
| RH | 0.000 - 0.007 | 0.030 | 1.180 | 242.90 |
| Y1 | 0.007 - 0.020 | 0.007 | 1.056 | 1163.40 |
| Y2 | 0.020 - 0.070 | 0.054 | 1.168 | 136.40 |
| Y3 | 0.070 - 0.200 | 0.260 | 1.172 | 28.20 |
| Y4 | 0.200 - 0.700 | 0.310 | 1.105 | 25.10 |
| I1 | 0.700 - 2.000 | 1.290 | 1.077 | 6.19 |
| I2 | 2.000 - 7.000 | 3.090 | 1.022 | 2.72 |
| G2 | > 10 | 8.600 | 1.000 | 1.00 |

## 2 BURST SIMULATIONS

The observational material for star clusters and galaxies consists of 12 Å resolution spectra in the range 3700–9700 Å, which were collected at La Silla, ESO and have been described in BA86a, BA87a and BA87b. The obtention of the composite starburst plus galaxy spectra, of the *BVRI* magnitudes and $W_\lambda$ for metallic and Balmer features was carried out with a spectral analysis package developed in Porto Alegre.

We have represented the red underlying populations by spectral groups E1 and E3 defined in Bica (1988). Spectral group E1 is an average of very strong-lined elliptical and S0 galaxy nuclei (e.g. NGC 4472). Spectral group E3 corresponds to red nuclei with weaker metallic features, as found in early-type galaxies of lower luminosity, $M_B \approx -20$ (e.g. NGC 4033). We point out that similar spectra are common among spiral galaxy bulges, the spectral type S1 being a counterpart of E1 and S3 of E3 (Bica 1988). Consequently, our simulations for nuclei in early-type galaxies can equally well represent events in the nuclei of spiral galaxies.

We show in Table 1 the properties of the star cluster spectral groups. In column 1 we recall the spectral group designations: RH stands for the H II region phase, Y for the young groups, I for the intermediate age groups and G for globular clusters. The corresponding age range is given in column 2. We provide in column 3 the $M/L_v$ ratio according to the star cluster theoretical models of Bica *et al.* (1988). Column 4 displays the $L_v/L$ (5870 Å) ratio relative to group G2, the old clusters with metallicity comparable to that of the younger groups; this ratio is an observed parameter used to transform *V* fluxes mutually into our adopted monochromatic flux normalization at 5870 Å. Finally, in the last column, we show the $L$(5870 Å) flux evolution for equal mass groups, relative to the oldest one. We point out that both our star cluster theoretical models and spectral library include the red supergiant phase which is responsible for the flux maximum in group Y1 at $\approx 10^7$ yr. Apart from this, the flux sequence merely represents the natural flux fading of a star cluster – or starburst – resulting from stellar evolution. The star cluster spectra for young and intermediate ages are from LMC and galactic disc clusters. Thus, they basically match star formation events from gas with less than or solar metallicity. Also, the single generation model in Arimoto & Bica (1989) has a value of $[Z/Z_\odot] = -0.30$. Considering instead bursts from gas with a high metal content, one must use synthetic clusters computed via model atmosphere stars. An alternative solution would be to use young metal-rich clusters from the inner arms of M31. A general remark can be made however: young metal-rich bursts are not expected to differ much from the ones we use, because hot stars

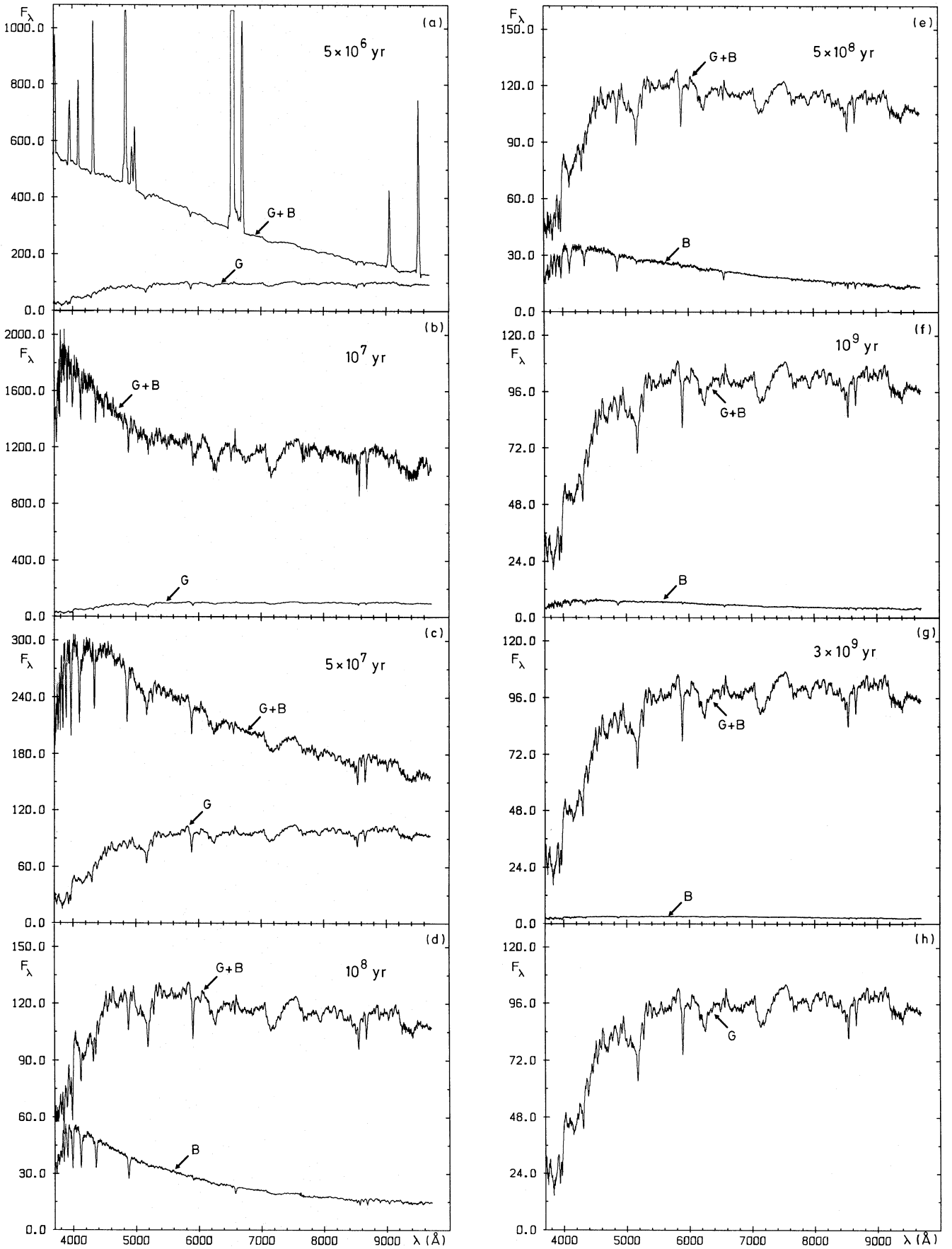


**Figure 1.** The age sequence of the composite burst plus galaxy spectrum for a burst mass of 1 per cent and group E1 as the underlying old population. In all figures the relative intensity scale corresponds to $F_\lambda = 100$ at 5870 Å for E1. The burst age is displayed in the upper right-hand corner.

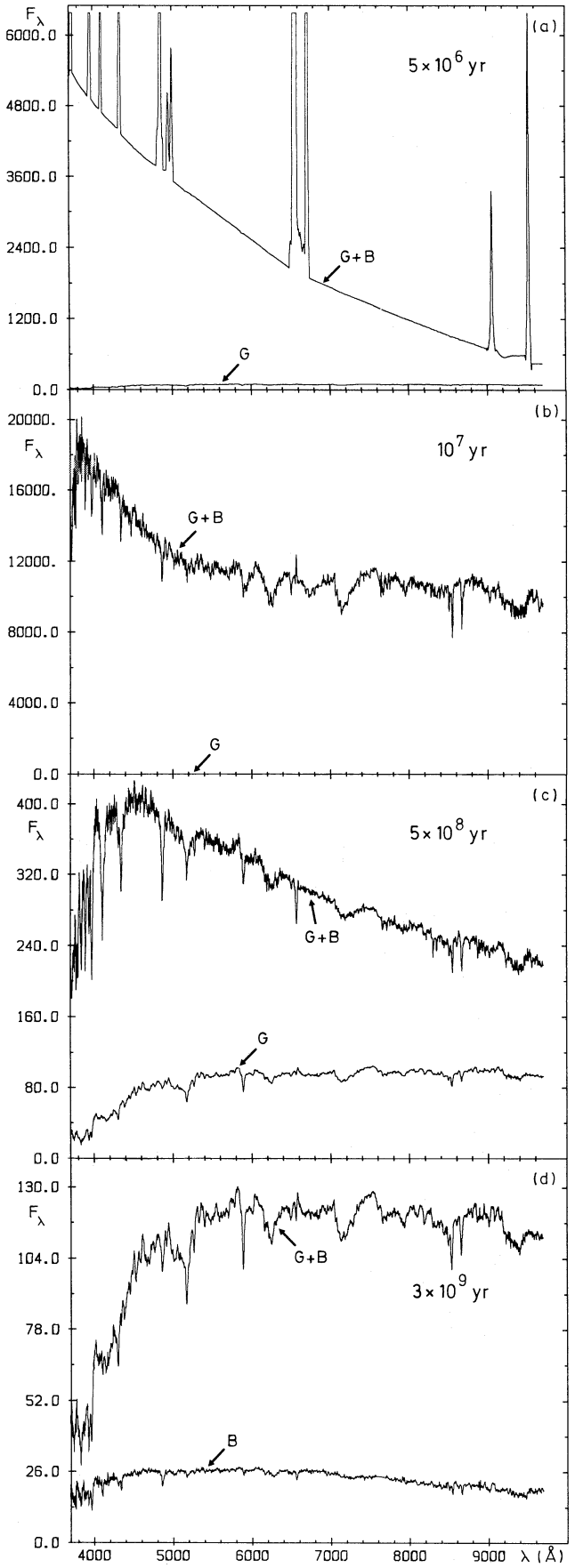


**Figure 2.** The effect of a 10 per cent mass burst with group E1 as the underlying population. Same intensity scale as in Fig. 1. The burst age is displayed in the upper right-hand corner.

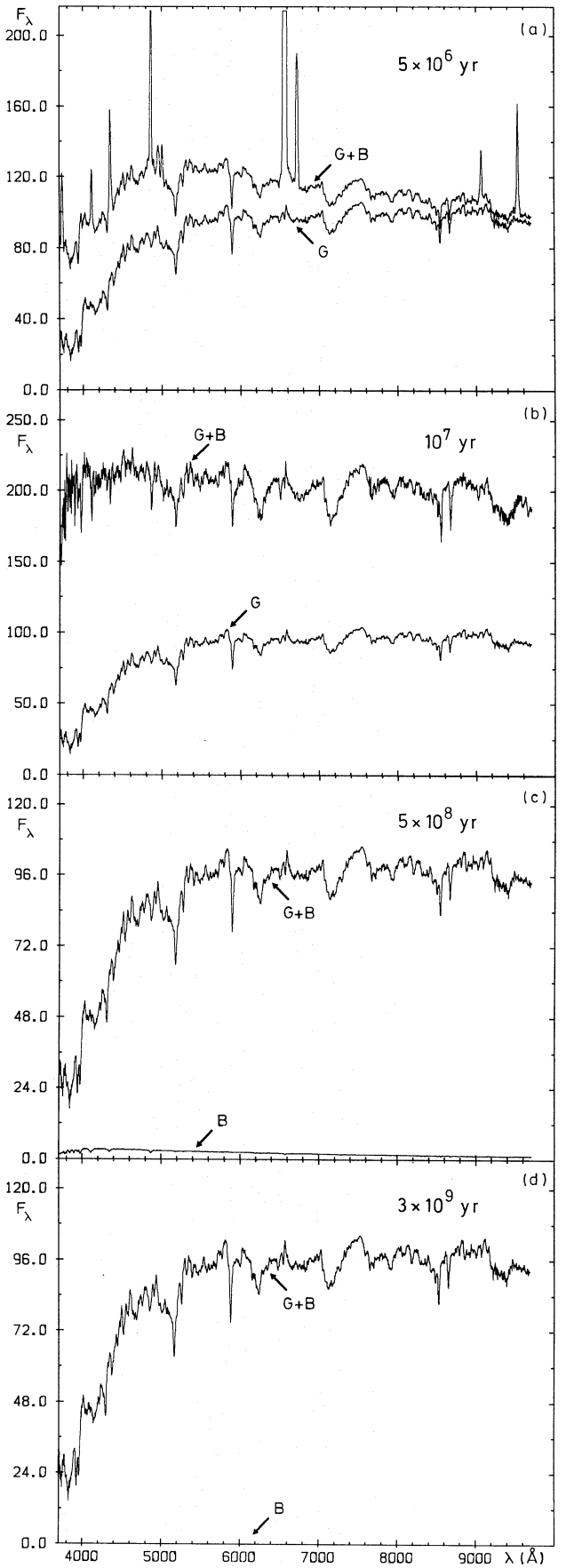


**Figure 3.** The effect of a 0.1 per cent mass burst with group E1 as the underlying population. Same intensity scale as in Fig. 1. The burst age is given in the upper right-hand corner.

**Table 2.** Colours and equivalent widths (Å) corresponding to the star cluster and galaxy spectra.

| Group | B-V | V-R | V-I | K CaII | H δ | H ϒ | H β | Mg+MgH | CaII 8542 | CaII 8662 |
|---|---|---|---|---|---|---|---|---|---|---|
| RH | 0.09 | 0.41 | 0.21 | -0.6 | -12.0 | -24.0 | -70.5 | 0.0 | 0.0 | 0.0 |
| Y1 | 0.36 | 0.50 | 1.31 | 2.0 | 4.2 | 3.3 | 4.1 | 3.0 | 6.4 | 5.5 |
| Y2 | 0.24 | 0.30 | 0.68 | 1.3 | 9.1 | 7.0 | 7.1 | 1.2 | 5.9 | 6.2 |
| Y3 | 0.25 | 0.27 | 0.64 | 2.4 | 10.0 | 8.6 | 8.0 | 1.7 | 5.8 | 5.6 |
| Y4 | 0.46 | 0.41 | 0.83 | 7.1 | 11.6 | 8.3 | 8.5 | 2.7 | 4.4 | 4.9 |
| I1 | 0.60 | 0.47 | 0.87 | 9.1 | 8.9 | 8.3 | 7.3 | 2.4 | 3.5 | 5.2 |
| I2 | 0.75 | 0.62 | 1.29 | 11.3 | 7.1 | 6.8 | 5.8 | 2.8 | 4.6 | 5.0 |
| E1 | 1.04 | 0.78 | 1.55 | 18.1 | 6.6 | 6.8 | 3.9 | 11.0 | 6.3 | 5.4 |
| E3 | 0.96 | 0.72 | 1.44 | 17.0 | 3.4 | 5.2 | 4.6 | 8.4 | 7.1 | 6.2 |

dominate the visible light and the opacity is not large. In the case of intermediate age bursts, red stars become increasingly important in the blue range, so the colours of such bursts should be redder and their spectral features stronger than for low-metallicity intermediate age bursts. We represent schematically the H II region phase by an absorption-featureless continuum derived from observed H II regions affected by internal reddening. Emission lines on top of this continuum are from an H II region galaxy nucleus. The value $W(H\beta) = 50$ Å in this spectrum corresponds to an H II region or a mixture of H II regions in the range $4.5-6 \times 10^6$ yr (Copetti, Pastoriza & Dottori 1986). This procedure allows one to observe the dilution of spectral features in the composite with an old population (Figs 1–3).

Starburst simulations consist of adding a star cluster spectrum at a given age (RH to I2 in Table 2) to that of a red galaxy nucleus (E1 or E3). They are related through the values given in column 5 of Table 1, where it has been assumed that the mass-to-light ratio of a red nucleus corresponds to that of the globular cluster group G2. Indeed, the population of red nuclei is dominated by the very old component (Bica 1988) and this assumption seems appropriate. At face value, the cluster group G2 has a mean metallicity $[Z/Z_\odot] = -0.40$, smaller than in the galaxy groups (E1 and E3) considered here. However, blanketing effects in the $V$ filter are quite small and consequently, the $M/L_v$ ratio depends very little on this parameter (Yoshii & Arimoto 1987).

We show in Fig. 1(a)–(g), the complete sequence of composite spectra for a 1 per cent burst-to-galaxy mass ratio and using the galaxy group E1 which corresponds to massive elliptical and S0 galaxy nuclei. In each figure we have displayed the composite spectrum and either that of the burst or of the underlying galaxy for clarity. In the H II region phase, the burst is dominant and it becomes even brighter during the red supergiant phase after about $10^7$ yr. Then, the burst fades away and the underlying old population becomes conspicuous again after $10^8$ yr. When the starburst turns from blue to red at approximately $5 \times 10^8$ to $10^9$ yr, Balmer lines are enhanced with respect to the pure old population. Finally, when the burst reaches an intermediate age (Fig. 1g), its contribution has become negligible.

The influence of the burst strength is shown in Figs 2 and 3, respectively, for burst-to-galaxy mass ratios of 10 and 0.1 per cent, at a selection of burst ages. For a 10 per cent mass burst, the underlying old population remains undetectable, at least by means of integrated spectra, over the first $5 \times 10^7$ yr. Its effect is so large that, even when at intermediate ages, it is still conspicuous, producing 20 per cent of the optical flux (Fig. 2d). In the case of a 0.1 per cent mass burst, the signature of a young stellar component is visible in the composite spectrum for $2 \times 10^7$ yr (Fig. 3a and b). An interesting configuration occurs at the red supergiant phase, when the combination of the burst with the red underlying population results in a flat spectrum spotted with strong absorption

**Table 3.** (a) The colour and magnitude changes for a composite burst plus E1 galaxy system.

| G+B / % | B-V | V-R | V-I | δ B | δ V | δ R | δ I |
|---|---|---|---|---|---|---|---|
| E1+RH / 0.1 | 0.73 | 0.69 | 1.32 | -0.61 | -0.30 | -0.22 | -0.07 |
| E1+Y1 / 0.1 | 0.61 | 0.62 | 1.42 | -1.33 | -0.90 | -0.75 | -0.77 |
| E1+Y2 / 0.1 | 0.88 | 0.71 | 1.45 | -0.33 | -0.17 | -0.10 | -0.07 |
| E1+Y3 / 0.1 | 1.00 | 0.76 | 1.52 | -0.08 | -0.04 | -0.02 | -0.01 |
| E1+Y4 / 0.1 | 1.02 | 0.77 | 1.53 | -0.05 | -0.03 | -0.02 | -0.02 |
| E1+I1 / 0.1 | 1.04 | 0.78 | 1.54 | -0.04 | 0.01 | -0.03 | -0.03 |
| E1+I2 / 0.1 | 1.04 | 0.78 | 1.55 | 0.00 | 0.00 | 0.00 | 0.00 |
| E1+RH / 1.0 | 0.26 | 0.50 | 0.64 | -2.34 | -1.55 | -1.28 | -0.66 |
| E1+Y1 / 1.0 | 0.40 | 0.52 | 1.33 | -3.50 | -2.86 | -2.60 | -2.64 |
| E1+Y2 / 1.0 | 0.48 | 0.49 | 1.06 | -1.64 | -1.07 | -0.78 | -0.59 |
| E1+Y3 / 1.0 | 0.78 | 0.65 | 1.36 | -0.59 | -0.33 | -0.20 | -0.14 |
| E1+Y4 / 1.0 | 0.88 | 0.70 | 1.41 | -0.44 | -0.28 | -0.20 | -0.14 |
| E1+I1 / 1.0 | 1.01 | 0.76 | 1.51 | -0.11 | -0.07 | -0.05 | -0.04 |
| E1+I2 / 1.0 | 1.03 | 0.77 | 1.54 | -0.04 | -0.03 | -0.03 | -0.02 |
| E1+RH / 10.0 | 0.11 | 0.42 | 0.27 | -4.72 | -3.79 | -3.43 | -2.52 |
| E1+Y1 / 10.0 | 0.36 | 0.50 | 1.31 | -5.97 | -5.29 | -5.01 | -5.05 |
| E1+Y2 / 10.0 | 0.27 | 0.33 | 0.74 | -3.90 | -3.13 | -2.68 | -2.33 |
| E1+Y3 / 10.0 | 0.39 | 0.39 | 0.89 | -2.29 | -1.64 | -1.25 | -0.98 |
| E1+Y4 / 10.0 | 0.58 | 0.51 | 1.05 | -1.94 | -1.48 | -1.22 | -0.99 |
| E1+I1 / 10.0 | 0.84 | 0.65 | 1.30 | -0.78 | -0.58 | -0.45 | -0.34 |
| E1+I2 / 10.0 | 0.97 | 0.74 | 1.49 | -0.35 | -0.28 | -0.24 | -0.22 |

**Table 3.** (b) Same as (a), but for a composite burst plus E3 galaxy system.

| G+B / % | B-V | V-R | V-I | δ B | δ V | δ R | δ I |
|---|---|---|---|---|---|---|---|
| E3+RH/0.1 | 0.69 | 0.65 | 1.23 | -0.57 | -0.29 | -0.22 | -0.08 |
| E3+Y1 /0.1 | 0.59 | 0.60 | 1.37 | -1.26 | -0.89 | -0.76 | -0.81 |
| E3+Y2 /0.1 | 0.82 | 0.67 | 1.36 | -0.30 | -0.17 | -0.11 | -0.08 |
| E3+Y3 / 0.1 | 0.92 | 0.71 | 1.42 | -0.07 | -0.04 | -0.02 | -0.02 |
| E3+Y4 / 0.1 | 0.94 | 0.72 | 1.43 | -0.05 | -0.03 | -0.02 | -0.02 |
| E3+I1 / 0.1 | 0.95 | 0.72 | 1.44 | -0.01 | -0.01 | -0.01 | -0.01 |
| E3+I2 / 0.1 | 0.96 | 0.72 | 1.44 | 0.00 | 0.00 | 0.00 | 0.00 |
| E3+RH / 1.0 | 0.25 | 0.49 | 0.61 | -2.24 | -1.54 | -0.32 | -0.52 |
| E3+Y1 / 1.0 | 0.39 | 0.52 | 1.32 | -3.40 | -2.84 | -2.63 | -2.71 |
| E3+Y2 / 1.0 | 0.46 | 0.47 | 1.02 | -1.55 | -1.06 | -0.80 | -0.63 |
| E3+Y3 / 1.0 | 0.73 | 0.61 | 1.27 | -0.55 | -0.32 | -0.21 | -0.15 |
| E3+Y4 / 1.0 | 0.83 | 0.66 | 1.33 | -0.40 | -0.27 | -0.21 | -0.16 |
| E3+I1 / 1.0 | 0.93 | 0.71 | 1.41 | -0.10 | -0.07 | -0.06 | -0.04 |
| E3+I2 / 1.0 | 0.95 | 0.72 | 1.44 | -0.04 | -0.03 | -0.03 | -0.03 |
| E3+RH / 10.0 | 0.11 | 0.42 | 0.26 | -4.61 | -3.77 | -3.46 | -2.59 |
| E3+Y1 / 10.0 | 0.36 | 0.50 | 1.31 | -5.86 | -5.26 | -5.04 | -5.13 |
| E3+Y2 / 10.0 | 0.27 | 0.33 | 0.74 | -3.79 | -3.10 | -2.71 | -2.40 |
| E3+Y3 / 10.0 | 0.38 | 0.38 | 0.86 | -2.20 | -1.62 | -1.27 | -1.04 |
| E3+Y4 / 10.0 | 0.57 | 0.49 | 1.02 | -1.86 | -1.47 | -1.24 | -1.04 |
| E3+I1 / 10.0 | 0.80 | 0.62 | 1.24 | -0.73 | -0.57 | -0.47 | -0.36 |
| E3+I2 / 10.0 | 0.91 | 0.70 | 1.41 | -0.32 | -0.27 | -0.25 | -0.24 |

The model designation (column 1) indicates the type of the underlying galaxy (E1 or E3), the starburst type (from RH to I2) and the respective mass proportion (burst/galaxy), as a percentage.

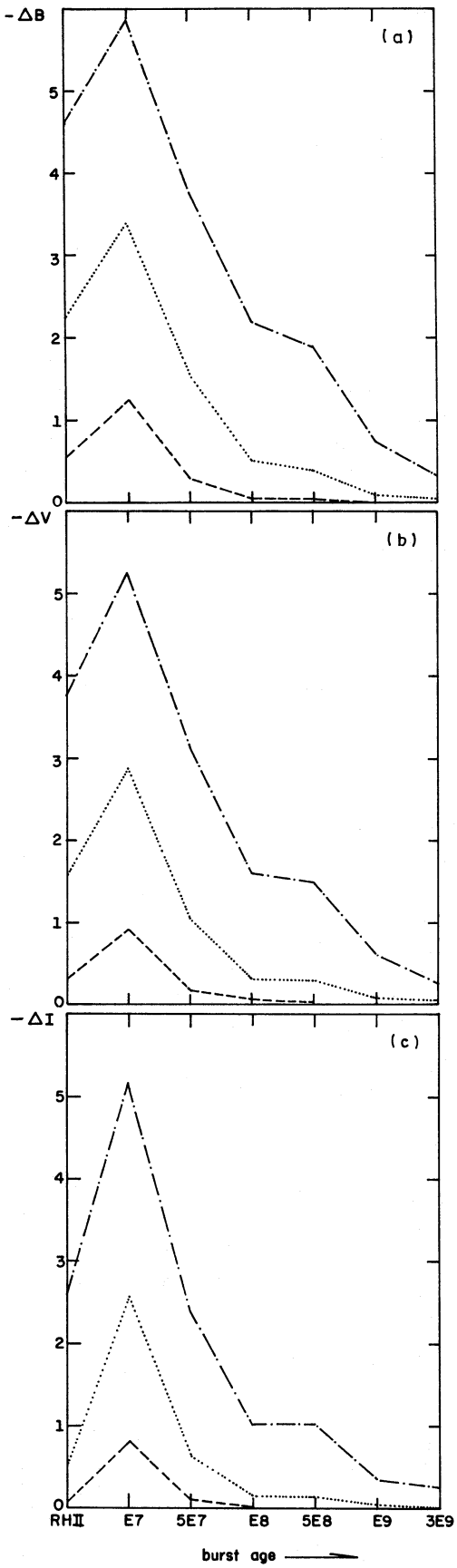


**Figure 4.** The magnitude changes induced by a starburst in an E3 galaxy for the *B*, *V* and *I* filters as a function of the burst age and strength. Dashed line: burst-to-galaxy mass ratio of 0.1 per cent; dotted line: ratio of 1 per cent; dash-dotted line: ratio of 10 per cent.

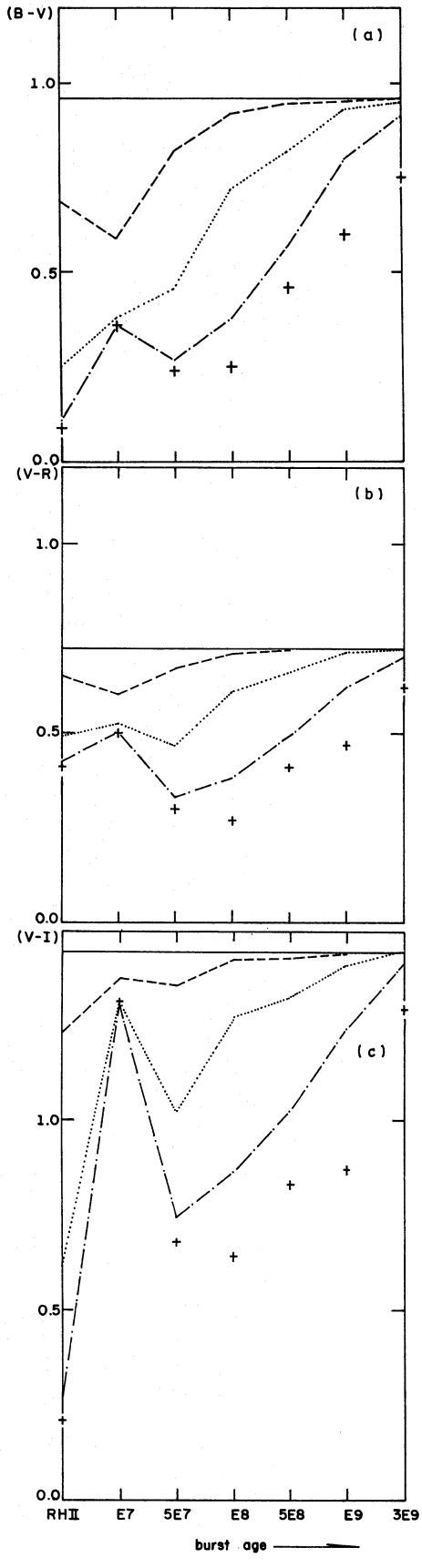


**Figure 5.** (*B*–*V*), (*V*–*R*) and (*V*–*I*) colours for a starburst on top of an E3 galaxy. Same symbols as in Fig. 4. Solid line: pure E3 colours; crosses; pure star burst (star cluster) colours.

features (Fig. 3b). However, such a configuration will be difficult to observe as it is certainly quite brief with respect to a burst duration: a mixture of the H II region and of the red supergiant phases should rather be expected. And last, a 0.1 per cent mass burst will become invisible as soon as it is $5 \times 10^8$ yr old.

## 3 *BVRI* MAGNITUDES AND COLOURS

In order to derive usual broad-band magnitudes and colours, we have convolved the resulting composite burst plus underlying galaxy spectra with the *B*, *V*, *R* and *I* filter responses. The results appear in Table 3 which provides the *B*, *V*, *R* and *I* magnitude changes when a starburst occurs on top of an underlying old population. The comparison between Tables 3(a) and (b) reveals the minor influence of a metallicity difference in the underlying populations E1 or E3, on the composite spectrum. The colours of star clusters and old population galaxy nuclei (E1 and E3) are given in Table 2.

In Fig. 4(a)–(c), we illustrate the change in magnitude, with respect to an E3 underlying population, of the composite starburst plus galaxy system, for a selection of 3 filters. The influence of the starburst draws a similar pattern in the various spectral ranges. Complementary to the analysis in Section 2, Fig. 4 clearly indicates when the effect of the starburst vanishes, which depends on the burst strength. We have displayed in Fig. 5(a)–(c), the colour changes of the composite burst plus galaxy system, as a function of the burst age and strength. We have also recalled the pure galaxy old population and the pure starburst (star cluster) colours. The starburst effect is quite prominent in the $(B-V)$ colours, while damped out in $(V-R)$, as the result of the larger sensitivity of the *B* filter to the presence of hot stars from the burst. The amplitude of the colour variations induced by a starburst is larger when a filter in the visible is compared to one in the near infrared (Fig. 5c) because the old population shows up more at larger wavelengths. However, it should be noted that a starburst at the red supergiant phase and a galaxy old population have similar $(V-I)$ colours, although they differ considerably in $(B-V)$.

## 4 EQUIVALENT WIDTHS OF SPECTRAL FEATURES IN THE COMPOSITE SYSTEMS

Following the window definitions and continuum tracings in BA86a, BA87b and BA88, we have measured the equivalent widths for a selection of metallic and Balmer lines in the composite burst plus galaxy spectra. Results are given in Tables 4a and 4b, respectively for underlying old populations E1 and E3. For comparison, we provide in Table 2 the equivalent widths of the same features for pure starbursts and pure galaxy old populations (E1 and E3). Some of these results are illustrated graphically in Fig. 6(a)–(c) and in Fig. 7 where we show the time evolution of three metallic features and H$\delta$. The effect of dilution due to blue stars in the burst is quite strong at Ca II K, even for a small mass burst (the 0.1 per cent case). At the Ca II infrared triplet, the dilution effect is important only during the H II region phase. For older ages of the starburst, metallicity is the parameter which rules the composite spectrum in the near infrared.

Regarding the Balmer H$\delta$ line, one can see that at early epochs of the starburst, the emission component from the H II region dominates. For older ages, the maximum $W_\lambda$ absorption value depends both on the burst age and strength. Other Balmer lines, presented in Table 4, exhibit similar behaviour.

If one now observes a composite spectrum, can the burst age be easily discriminated against its strength?

At early stages of the burst (age about $5 \times 10^6$ yr), the H II region phase is obvious and easily recognized through its strong emission lines. The absence of absorption features, in particular in the near infrared around the TiO bands and the Ca II triplet, implies that the burst strength is 10 per cent at least. A comparison between the spectral feature sets in absorption and in emission allows one to estimate in a rather precise way the burst strength (Figs 1a, 2a and 3a).

At the red supergiant phase within the burst (age about

**Table 4.** (a) Equivalent widths (Å) of prominent features for galaxy E1 plus burst composite spectra.

| G+B / % | K CaII | H δ | H ϰ | H β | Mg+MgH | CaII 8542 | CaII 8662 |
|---|---|---|---|---|---|---|---|
| E1+RH / 0.1 | 8.2 | -1.9 | -4.7 | -17.5 | 8.2 | 5.8 | 5.0 |
| E1+Y1 / 0.1 | 5.0 | 4.8 | 4.4 | 3.9 | 6.4 | 6.4 | 5.5 |
| E1+Y2 / 0.1 | 11.8 | 7.4 | 6.9 | 4.5 | 9.6 | 6.3 | 5.5 |
| E1+Y3 / 0.1 | 16.4 | 6.9 | 6.9 | 4.1 | 10.7 | 6.3 | 5.5 |
| E1+Y4 / 0.1 | 17.4 | 6.9 | 6.9 | 4.1 | 10.8 | 6.3 | 5.5 |
| E1+I1 / 0.1 | 18.0 | 6.6 | 6.8 | 3.9 | 10.9 | 6.3 | 5.5 |
| E1+I2 / 0.1 | 18.1 | 6.6 | 6.9 | 3.9 | 11.0 | 6.3 | 5.5 |
| E1+RH / 1.0 | 1.0 | -10.0 | -19.6 | -55.8 | 2.5 | 3.3 | 2.8 |
| E1+Y1 / 1.0 | 2.4 | 4.3 | 3.5 | 4.1 | 3.6 | 6.4 | 5.5 |
| E1+Y2 / 1.0 | 3.7 | 8.7 | 6.9 | 6.1 | 5.0 | 6.1 | 5.8 |
| E1+Y3 / 1.0 | 9.4 | 8.3 | 7.6 | 5.2 | 8.5 | 6.2 | 5.5 |
| E1+Y4 / 1.0 | 13.5 | 8.5 | 7.3 | 5.1 | 9.1 | 6.1 | 5.4 |
| E1+I1 / 1.0 | 17.0 | 6.9 | 7.0 | 4.1 | 10.4 | 6.2 | 5.4 |
| E1+I2 / 1.0 | 17.8 | 6.6 | 6.8 | 4.0 | 10.8 | 6.3 | 5.4 |
| E1+RH / 10.0 | -0.4 | -11.7 | -23.4 | -68.7 | 0.4 | 0.3 | 0.3 |
| E1+Y1 / 10.0 | 2.0 | 4.3 | 3.4 | 4.1 | 3.1 | 6.4 | 5.5 |
| E1+Y2 / 10.0 | 1.6 | 9.1 | 7.0 | 7.0 | 2.1 | 6.0 | 6.2 |
| E1+Y3 / 10.0 | 3.6 | 9.7 | 8.4 | 7.3 | 3.6 | 6.0 | 5.6 |
| E1+Y4 / 10.0 | 8.4 | 10.9 | 8.0 | 7.5 | 5.0 | 5.2 | 5.1 |
| E1+I1 / 10.0 | 12.7 | 7.9 | 7.6 | 7.1 | 7.4 | 5.5 | 5.4 |
| E1+I2 / 10.0 | 15.8 | 6.7 | 6.8 | 4.3 | 9.2 | 6.0 | 5.4 |

**Table 4.** (b) Equivalent widths (Å) of prominent features for galaxy E3 plus burst composite spectra.

| G+B / % | K CaII | H δ | H ϰ | H β | Mg+MgH | CaII 8542 | CaII 8662 |
|---|---|---|---|---|---|---|---|
| E3+RH / 0.1 | 8.5 | -3.1 | -5.4 | -16.5 | 6.3 | 6.5 | 5.7 |
| E3+Y1 / 0.1 | 5.4 | 4.0 | 3.9 | 4.3 | 5.4 | 6.7 | 5.9 |
| E3+Y2 / 0.1 | 11.7 | 5.1 | 5.6 | 5.0 | 7.4 | 7.0 | 6.2 |
| E3+Y3 / 0.1 | 15.6 | 3.9 | 5.4 | 4.8 | 8.2 | 7.1 | 6.2 |
| E3+Y4 /0.1 | 16.4 | 3.8 | 5.3 | 4.7 | 8.3 | 7.0 | 6.2 |
| E3+I1 / 0.1 | 16.9 | 3.5 | 5.2 | 5.0 | 8.4 | 7.1 | 6.2 |
| E3+I2 / 0.1 | 16.9 | 3.4 | 5.2 | 4.6 | 8.4 | 7.1 | 6.2 |
| E3+RH /1.0 | 1.1 | -10.1 | -19.6 | -55.2 | 2.0 | 3.7 | 3.1 |
| E3+Y1 / 1.0 | 2.4 | 4.2 | 3.4 | 4.2 | 3.4 | 6.5 | 5.6 |
| E3+Y2 / 1.0 | 3.9 | 8.0 | 6.6 | 6.3 | 4.1 | 6.6 | 6.2 |
| E3+Y3 / 1.0 | 9.6 | 6.4 | 6.6 | 5.6 | 6.6 | 6.9 | 6.1 |
| E3+Y4 / 1.0 | 13.3 | 6.3 | 6.2 | 5.6 | 7.2 | 6.7 | 6.0 |
| E3+I1 / 1.0 | 16.0 | 4.0 | 5.5 | 5.1 | 8.0 | 6.9 | 6.2 |
| E3+I2 / 1.0 | 16.7 | 3.5 | 5.3 | 4.7 | 8.3 | 7.0 | 6.2 |
| E3+RH / 10.0 | -0.4 | -11.7 | -23.4 | -68.6 | 0.3 | 0.4 | 0.4 |
| E3+Y1 / 10.0 | 2.0 | 4.3 | 3.4 | 4.1 | 3.0 | 6.4 | 5.6 |
| E3+Y2 / 10.0 | 1.6 | 9.0 | 6.9 | 7.0 | 2.0 | 6.1 | 6.2 |
| E3+Y3 / 10.0 | 3.7 | 9.3 | 8.2 | 7.4 | 3.1 | 6.3 | 5.8 |
| E3+Y4 / 10.0 | 8.5 | 10.3 | 7.7 | 7.6 | 4.3 | 5.4 | 5.4 |
| E3+I1 / 10.0 | 12.6 | 6.3 | 6.7 | 5.8 | 6.0 | 6.0 | 5.9 |
| E3+I2 / 10.0 | 15.3 | 4.4 | 5.6 | 4.9 | 7.2 | 6.6 | 6.0 |

Column 1: same meaning as in Table 3.

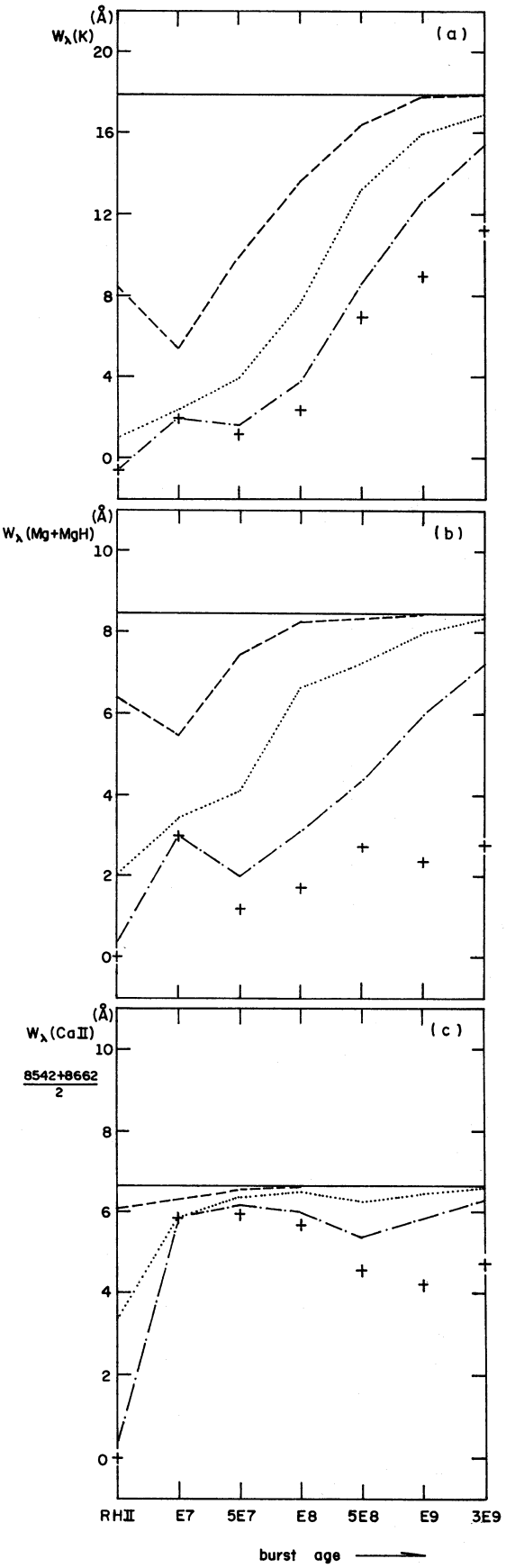


**Figure 6.** Evolution with time of the equivalent width of metallic features from the composite spectrum, burst plus E3 galaxy. Same symbols as in Fig. 5.

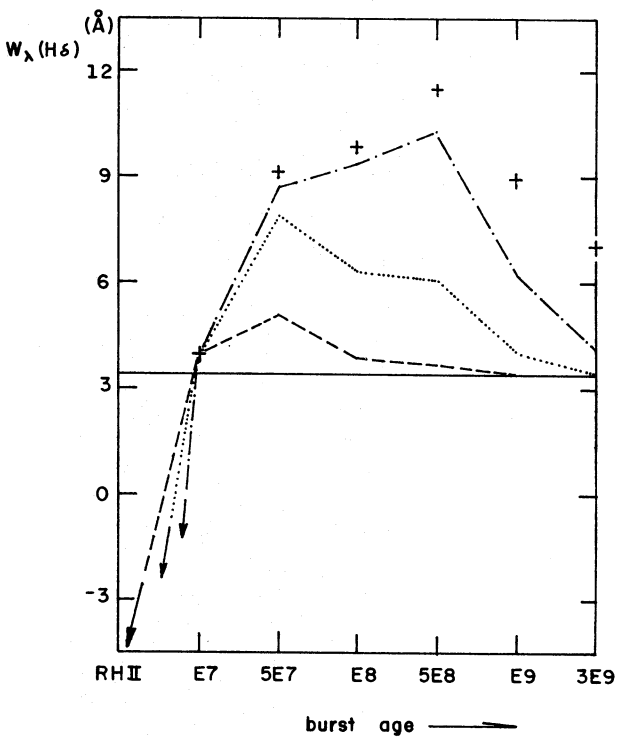


**Figure 7.** Evolution with time of the equivalent width of Hδ from the composite spectrum, burst plus E3 galaxy. Same symbols as in Fig. 5.

$10^7$ yr), the burst light dominates and produces a characteristic spectrum. At this stage, the burst strength changes the slope of the continuum in the composite spectrum, giving a flat spectrum for a 0.1 per cent burst and a blue rising spectrum for both the 1 and 10 per cent burst strengths.

Later, when the age burst reaches $5 \times 10^8$ yr and is recognized through a strong absorption Balmer series, the burst strength can also be roughly estimated. Only burst strengths larger than 1 per cent will still contaminate the underlying old population. In this case, the burst strength affects considerably the continuum shape: the larger it is, the bluer the composite continuum.

## 5 CONCLUDING REMARKS

The most common sources of gas available for star-forming events are found in galactic spiral discs and in Magellanic irregular galaxies. Thus, as the star clusters used for matching starbursts in these simulations are LMC clusters and galactic open clusters, our results can directly account for most of the major star-forming events. The underlying galaxy populations we have used (early-type groups E1 and E3), are identical to the populations found in red spiral nuclei (groups S1 and S3 in Bica 1988). Therefore, the models we have computed could equally describe star formation resulting from gas inflow from the disc to the nucleus of a spiral galaxy. Under some assumptions, they might also be used for explaining interaction-induced starbursts with gas transfer from spiral discs or irregular systems to older population galaxies.

The simulations describe the present state of the composite burst plus galaxy system, for starbursts having occurred

at the indicated age. They can also represent the starburst evolution in distant galaxies, if the underlying population is so old indeed that the effects of its own evolution are negligible.

We have deduced from the composite burst plus galaxy simulations, *B*, *V*, *R* and *I* magnitudes and colours, as well as a set of equivalent width measurements for metallic features and Balmer lines, to be used as diagnostics. They allow us to date and to estimate the strength of the starburst in star-forming systems. We have concluded in particular, that for a massive starburst, involving 10 per cent of the galaxy mass, the underlying old population will remain hidden during $5 \times 10^7$ yr, as long as integrated spectral observations are concerned. Although it is fundamental to know whether young galaxies exist in the present universe (e.g. Searle & Sargent 1972), our spectral simulations clearly demonstrate how difficult it will be to identify genuine young galaxies, in the sense of an isolated single generation star-forming object. At intermediate ages ($10^9$ yr), a massive starburst within an old galaxy will still contribute around 20 per cent of the total visible flux, while a 1 per cent mass burst will be barely detectable. Finally, a small starburst (0.1 per cent mass fraction) will affect the underlying galaxy spectrum for $2 \times 10^7$ yr only.

## ACKNOWLEDGMENTS

EB and AS acknowledge the Brazilian institution CNPq for their research fellowships.

## REFERENCES

Arimoto, N. & Bica, E., 1989. *Astr. Astrophys.*, **222, 89.**
Arimoto, N. & Yoshii, Y., 1986. *Astr. Astrophys.*, **164,** 260.
Bica, E., 1988. *Astr. Astrophys.*, **195,** 76.
Bica, E. & Alloin, D., 1986a. *Astr. Astrophys.*, **162,** 21.
Bica, E. & Alloin, D., 1986b. *Astr. Astrophys. Suppl.*, **66,** 171.
Bica, E. & Alloin, D., 1987a. *Astr. Astrophys.*, **70,** 281.
Bica, E. & Alloin, D., 1987b. *Astr. Astrophys.*, **186,** 49.
Bica, E. & Alloin, D., 1988. In: *Towards Understanding Galaxies at Large Redshifts*, p. 77, eds Kron, R. & Renzini, A., Kluwer Academic Publishers, Dordrecht.
Bica, E., Arimoto, N. & Alloin, D., 1988. *Astr. Astrophys.*, **202,** 8.
Copetti, M., Pastoriza, M. & Dottori, H., 1986. *Astr. Astrophys.*, **156,** 111.
Dennefeld, M., Karoji, H. & Belford, P., 1985. In: *Star-forming Dwarf Galaxies,* p. 351, eds Kunth, D., Thuan, T. X. & Tran Thanh Van, J., Editions Frontières, Gif sur Yvette.
Larson, R. & Tinsley, B., 1977. *Astrophys. J.*, **219,** 46.
Lequeux, J., Peimbert, M., Rayo, J., Serrano, A. & Torres-Peimbert, S., 1979. *Astr. Astrophys.*, **80,** 155.
Lonsdale, C. J., Persson, S. E. & Matthews, K., 1984. *Astrophys. J.*, **287,** 95.
Searle, L. & Sargent, W. L., 1972. *Astrophys. J.*, **173,** 25.
Searle, L., Sargent, W. L. & Bagnuolo, W., 1973. *Astrophys. J.*, **179,** 427.
Terlevich, R. J., 1985. In: *Star-forming Dwarf Galaxies*, p. 395, eds Kunth, D., Thuan, T. X. & Tran Thanh Van, J., Editions Frontières, Gif sur Yvette.
Thuan, T. X., 1983. *Astrophys. J.*, **268,** 667.
Wright, G. S., Joseph, R. D., Robertson, N. A., James, P. A. & Meikle, W. P., 1988. *Mon. Not. R. astr. Soc.*, **233,** 1.
Yoshii, Y. & Arimoto, N., 1987. *Astr. Astrophys.*, **188,** 13.